Cu_{2}S_{3} complex on Cu(111) as a candidate for mass transport enhancement

Holly Walen, Da-Jiang Liu, Junepyo Oh, Hyunseob Lim, J. W. Evans, Christine M. Aikens, Yousoo Kim, and P. A. Thiel

Phys. Rev. B **91**, 045426 — Published 22 January 2015

DOI: 10.1103/PhysRevB.91.045426

A New Sulfur-Metal Complex on Cu(111) as a Candidate for Mass Transport Enhancement

Holly Walen,[1] Da-Jiang Liu,[2] Junepyo Oh,[3] Hyunseob Lim,[3,†] J. W. Evans,[2,4] Christine Aikens,[5] Yousoo Kim,[3] and P. A. Thiel[1,2,6,*]

[1]Department of Chemistry, Iowa State University, Ames, Iowa 50011 USA
[2]Ames Laboratory of the USDOE, Ames, Iowa 50011 USA
[3]RIKEN Surface and Interface Science Laboratory, Wako, Saitama 351-0198, Japan
[4]Department of Physics & Astronomy, Iowa State University, Ames, Iowa 50011 USA
[5]Kansas State University, Department of Chemistry, Manhattan, Kansas 66506 USA
[6]Department of Materials Science & Engineering, Iowa State University, Ames, Iowa 50011 USA

Abstract

Sulfur-metal complexes, containing only a few atoms, can open new, highly efficient pathways for transport of metal atoms on surfaces. For example, they can accelerate changes in the shape and size of morphological features, such as nanoparticles, over time. In this study, we perform STM under conditions that are designed to specifically isolate such complexes. We find a new, unexpected S-Cu complex on the Cu(111) surface, which we identify as Cu_2S_3**.** We propose that Cu_2S_3 enhances mass transport in this system, which contradicts a previous proposal based on Cu_3S_3. We analyze bonding within these Cu-S complexes, identifying a new principle for stabilization of sulfur complexes on coinage metal surfaces.

Introduction.

It has been proposed that metal-adsorbate complexes can greatly accelerate rearrangements of metal nanostructures and surfaces. This issue is of importance for stability of catalysts or nanostructures, and has been the subject of prolonged speculation given that the complexity of such systems typically precludes definitive analysis [1,2]. Nonetheless, evidence continues to accumulate supporting the presence of mobile complexes on surfaces and, by implication, their role in metal transport. Recently, for instance, Parkinson et al. have shown that CO interacts with Pd atoms adsorbed on a Fe_3O_4 surface, forming a highly-mobile Pd-CO complex [3]. Other adsorbates that form mobile surface complexes with metals include hydrogen [4,5], oxygen [6,7], alkylsulfides [8], and—the subject of this study—sulfur [9-14]. The soft metals Cu, Ag, and Au, which are of great interest because of their catalytic and plasmonic properties, are expected to be particularly susceptible to this effect.

The challenge in identifying such complexes is their high mobility, plus their potential condensation into extended ordered structures at moderate to high coverage. Together, these considerations mean that conditions of low temperature and low coverage offer the best chance for isolating and observing such species. The present work is a search for S-Cu complexes under these conditions.

Previously, Feibelman [9] proposed that a Cu_3S_3 complex can enhance metal transport on Cu(111), not because of high mobility (relative to metal adatoms), but rather because of high population (reflecting high stability), combined with moderate mobility (cf. Ref. [1]). The stability of the cluster was attributed to the fact that S atoms could adsorb at pseudo-4-fold-

hollow (p4fh) sites created at the edges of the metal trimer, in accord with a long-standing principle that S binds more strongly to higher-coordination sites [9,15,16]. This conjecture seemed compatible with later experimental work [10], where coarsening kinetics of Cu islands above room temperature, in the presence of adsorbed S, were interpreted in terms of Feibelman's model. However, the Cu_3S_3 clusters were not observed directly.

In this paper, we present direct evidence for an abundant small cluster that is not Cu_3S_3, but rather Cu_2S_3, on Cu(111). This cluster is immobile and stable at 5 K, where our observations are made. It forms when the Cu(111) surface is exposed to sulfur at room temperature and then quenched. Thus, it is likely to exist and participate in dynamic processes that occur at higher temperature.

2. Experimental and computational details.

All STM imaging was done at 5 K in vacuum, at a pressure lower than 2.5×10^{-11} Torr [17]. Assessment of the sulfur coverage, θ_S, [the ratio of S atoms to Cu atoms in the (111) plane] was guided by the prior observation that a honeycomb-like reconstruction first appears at $\theta_S \sim 0.05$ [18,19]. We report S coverage on the terraces, rather than the total S coverage (which includes step decoration).

DFT calculations for surfaces used the VASP [20] code with the projector-augmented wave (PAW) method [21]. The surface was modeled by a periodic slab of L layers, separated by 1.2 nm of vacuum. Additional Cu and S atoms were added to one side of the slab. Most of the results reported used the Perdew-Burke-Ernzerhof (PBE) approximation [22] for the exchange-correlation functional. The energy cutoff for the plane-wave basis set was 280 eV. Simulated STM images are created from DFT calculations using the Tersoff-Hamman method [23,24]. Due to the existence of surface states on the Cu(111) surface, k-points convergence is slow. Averaging results for slabs of different thickness can significantly reduce the errors due to insufficient k-points. Energetics reported in this paper are obtained from k-point grids that approximately correspond to (24×24×1) for the primitive cell, averaging results from L = 4 to 7. Some key results were reproduced using DFT codes with dispersion interactions, e.g., DFT-D2 and optB88-vdW. Compared with PBE, absolute values were shifted by as much as 0.20 eV, but trends were preserved.

DFT calculations on gas phase CuS_2 and Cu_2S_3 molecules with varying charge states were performed with the Amsterdam Density Functional (ADF) code [25]. In the ADF program, the PBE functional [22] and a triple-zeta polarized (TZP) basis set with the frozen core approximation were used for geometry optimizations and Kohn-Sham orbital calculations. Relativistic effects were considered using the zeroth order regular approximation (ZORA) [26,27].

3. Identification of a Cu_2S_3 complex from STM and DFT.

The inset in Fig. 1(a) shows an image of the clean Cu(111) surface with atomic resolution. This allows us to define crystallographic directions as shown, with arrows indicating two of the six close-packed directions.

Fig. 1(a) shows a representative image of S/Cu(111) terraces at relatively low magnification, and at $\theta_S = 0.004$. At this low coverage, the main features are small, uniform bright spots. Closer inspection reveals that these are actually heart-shaped clusters, as shown in Fig. 1(c-e). They adopt three different orientations, rotated by 120^o, in equal abundance. These

orientations are such that the lobes of the heart align with three of the six close-packed directions of the Cu(111) surface.

We can identify the orientations of the hearts more exactly by using step edges as reference. There are two types of close-packed step edges in an fcc system. These are commonly denoted A and B, where A is a (100) microfacet exposing p4fh sites, and B is a (111) microfacet exposing p3fh sites. In experiment, both types of steps exist on the clean surface and they are not easily distinguishable. Sulfur adsorbs preferentially at steps and fully decorates the steps, even at lowest θ_S, in our experiments. After adsorption of sulfur, one type of step is long and straight, as exemplified in Fig. 2(a), while the other has a faceted sawtooth structure, as shown in Fig. 2(b) [18,19]. Notably, the inner edges of the sawtooth have the same orientation as the more extended, straight steps. We identify the straight steps as A-steps because these naturally present p4fh adsorption sites where S is more stable. Using this as reference, our STM images show that the heart-shaped clusters are oriented *exclusively* with their lobes toward downgoing B-steps.

We attribute the hearts to Cu_2S_3 clusters of the type shown in Fig. 3(a). There is one S atom on the upper side of the Cu dimer in the figure, in a p4fh site formed by the Cu dimer plus two Cu atoms in the terrace. There are two S atoms on the lower side of the Cu dimer, each near a 3fh site on the terrace and adjoining one of the Cu atoms in the dimer. These would shape the lobes of the heart.

We have used density functional theory (DFT) to check whether this assignment is reasonable in terms of stability, shape, orientation, and density. A variety of possible adsorbed clusters, with optimized configurations, are represented in Fig. 3. The chemical potential of S (μ_S) and the cluster diffusion barrier (E_d) appear at the top of each panel. μ_S is defined as:

$$\mu_S = [E(Cu_mS_n + slab) - E(slab) - m\,\mu_{Cu}]/n - E(S_{2,g})/2 \qquad (1)$$

where E is energy, μ_{Cu} is the cohesive energy of a bulk Cu atom, and m and n are the number of Cu and S atoms in the complex, respectively. By this definition, μ_S measures the decrease in energy per S when a limited supply of atomic S on terraces is incorporated into clusters (given an unlimited supply of metal atoms available from steps). This equation also defines the energy of gaseous S_2 as the reference point for μ_S.

A related quantity, the formation energy, E_{form}, is defined by:

$$E_{form}(Cu_mS_n) = n[\mu_S(Cu_mS_n) - \mu_S(S)] \qquad (2)$$

E_{form} gives the energy cost to create a Cu_mS_n complex by extracting m Cu atoms from the step edge and combining them with n S atoms already on the terrace. However, Eq. (2) includes $\mu_S(S)$, which varies with θ_S. Since we are dealing with low θ_S, we choose the value of $\mu_S(S)$ that is calculated from DFT for a "large" 4x4 supercell, corresponding to $\theta_S = 0.0625$ ML, which is $\mu_S(S) = -1.91$ eV. The sulfur atoms are in fcc sites. This results in the values of E_{form} shown in Table 1 for the optimized configurations of several Cu-S complexes. To facilitate comparisons, the values of μ_S and E_d are also shown.

Table 1. Energetic values calculated from VASP for optimized configurations of several Cu-S complexes, and an isolated Cu atom, on Cu(111).

Complex	μ_S	E_d	E_{form}, eV
Cu atom at an fcc terrace site	n/a	0.05	+0.78
CuS	-1.24	0.33	+0.67
CuS_2	-1.82	0.34	+0.15
CuS_3	-1.83	0.36	+0.24
Cu_2S_3	-1.87	0.35	+0.11
Cu_3S_3	-1.82	0.36	+0.24

The Cu_2S_3 complex in Fig. 3(a) has lower μ_S than any others we have found. The 3 next-best complexes are shown Fig. 3(c-e). However, the ordering of μ_S for various complexes can be sensitive to the dimension and orientation of the supercell, meaning that lateral interactions between complexes can affect the relative energies significantly. These are best taken into account by comparing μ_S, not at fixed supercell size as in Fig. 3, but rather at fixed θ_S, as in Fig. 4. At all θ_S, μ_S of Cu_2S_3 is lower than μ_S of Cu_3S_3, and at most coverages, it is below μ_S of atomic adsorbed S.

Second, we have simulated the shape of the complexes using the Tersoff-Hamman method [23,24]. Results are shown in Fig. 5, where panels (a) and (b) correspond to the configurations shown in Fig. 3(a) and 3(c), respectively. The heart shape is evident for Cu_2S_3, whereas Cu_3S_3 is three-fold symmetric and incompatible with the data. Furthermore, the area of the simulated Cu_2S_3 complex is 0.40-0.42 nm^2, in good agreement with the experimental result (0.39 ± 0.04 nm^2).

Third, to assess orientation, we contemplate the two Cu_2S_3 complexes shown in Fig. 3(a-b). The one in Fig. 3(a) can have 3 energetically-equivalent orientations. In each orientation, there is one S atom in a p4fh site and two S atoms in asymmetrical sites. Considering the pair of Cu atoms as a one-dimensional step edge, one S atom lies along an A-step, and the others (comprising the lobes) are along a B-step. This is exactly the experimental observation. On the other hand, the complex in Fig. 3(b) has one S atom along a B-step, and the lobes along an A-step, inconsistent with the data. The stability of complex (a) can be rationalized by the presence of one S atom in a p4fh site, whereas (b) has none.

Finally, we considered whether the observed density of complexes is consistent with our analysis of the above energetics. A simple Boltzmann factor analysis given the positive formation energy implies that the density predicted under preparation conditions at 300 K should exceed the static density observed at the lower observation temperature (5 K). (The density observed at 5 K should reflect the equilibrium density for the temperature at which the complexes are frozen in place during cooling. This freeze-in temperature lies between 300 K and 5 K, but is otherwise unknown.) The formation energy for Cu_2S_3 is +0.11 eV, so the equilibrium population predicted at 300 K is $0.25/nm^2$. This is well above the observed value of $0.02/nm^2$. Hence the two values are consistent.

4. Factors that stabilize Cu-S complexes.

The existence of Cu_2S_3 complexes is surprising, given that analogous clusters have not been observed (to our knowledge) in other surface systems. To understand why they exist, we

first recall the well-known principle governing S adsorption on metal surfaces is that S bonds preferentially at 4fh sites, and in some cases metal surfaces rearrange to provide such sites [16]. The stability of the (hypothetical) Cu_3S_3 complex, for instance, was attributed to S atoms occupying three p4fh sites at the edges of the metal trimer [9] [Fig. 3(c)]. However, in the Cu_2S_3 cluster, two of the p4fh sites are sacrificed by virtue of the missing Cu atom. Thus, a factor must exist that competes with, or complements, the influence of the 4fh site. We suggest that this is the formation of linear S-Cu-S units. The Cu_2S_3 complex consists of two such linear units, sharing a S atom at the apex. Adding a Cu atom to form Cu_3S_3 breaks the linearity of the individual S-Cu-S units, as can be discerned in Fig. 3(c).

Insight into this configuration can be developed by starting with the isolated CuS_2 molecule, where we define the z-axis as the internuclear axis. In a linear ligand field, the Cu d orbitals split into two doubly-degenerate orbitals, (d_{x2-y2}, d_{xy}) and (d_{xz}, d_{yz}), and a nondegenerate d_{z2} orbital. Of these, the d_{z2} orbital is positioned for the best overlap with ligand s or p orbitals, followed by the (d_{xz}, d_{yz}) set and finally the essentially nonbonding (d_{x2-y2}, d_{xy}) set.

The calculated Kohn-Sham molecular orbitals for CuS_2^- at the PBE/TZP level of theory agree with this picture. Kohn-Sham orbitals for CuS_2 are shown in Fig. 6 (the -3 charge state is shown here; different charge states vary in their occupation of the HOMO). The lowest energy orbital shown here (HOMO-6) is a bonding interaction between the Cu d_{z2} orbital and the S $2p_z$ orbitals. π-like orbitals between Cu d_{xz} and d_{yz} and the corresponding S $2p_x$ and $2p_y$ atomic orbitals also aid in the strong bonding interaction. In Cu_2S_3, the Kohn-Sham orbitals are more delocalized, but still fit with the CuS_2 picture.

Hence, linearity of the S-Cu-S unit is favored in isolated molecules because it maximizes overlap between Cu d_{z2} and S $2p_z$ orbitals. Analysis of VASP-based isodensity plots of adsorbed Cu-S complexes reveals that this trend is preserved on the surface. The isodensity plots for CuS_2 generated from VASP (Fig. 7) show similar results for the lowest energy orbitals. Isodensity plots for states 3 and 4 for one Cu layer (L=1) display the bonding and antibonding configurations of the CuS_2 HOMO-6 orbital with the Cu substrate. A small energy splitting indicates that there is a weak interaction between this orbital and the Cu substrate. Isodensity plots for states 5 and 6 for L=1 show bonding interactions between S 2p orbitals that are perpendicular to the plane of the Cu surface and the underlying Cu layer. This indicates that the stability of the CuS_2 units on the surface can be understood both in terms of the S-Cu-S interactions and the S-surface interactions. Isodensity plots for Cu_2S_3 in vacuum and on one layer of Cu substrate are shown in Fig. 8. The 2p orbitals of the S atom at the apex have a different symmetry than those of the rest of the S atoms in the complex. One S 2p orbital is perpendicular to the Cu atoms within the complex, the lower lobe of which interacts with the two Cu d_{z2} S p_z orbitals, shown as vacuum state 4 in Fig. 8. Another S 2p orbital is parallel to the Cu atoms in the complex, and each lobe interacts separately with the Cu d_{z2} S p_z orbitals, shown as vacuum state 5 in Fig. 8. These bonding interactions are also present for the complex on one Cu layer. The states 4 and 5 in vacuum become states 5 and 6 with L=1. In addition, low energy states exhibit isodensity plots with significant S 2p character perpendicular to the surface (e.g., the L=1 state 4 in Fig. 8. Again, the stability of Cu_2S_3 is represented by the linear S-Cu-S interactions and the S-surface interactions.

In fact, linear S-M-S units are known in some related systems. Thiolates adsorbed on Au(111) [8,28], and thiolates at the periphery of Au nanoclusters, form species that include linear S-M-S units [28,29]. Linear S-M-S complexes (without alkyl ligands) have also been postulated—but not observed directly—on the basis of DFT and experimental data for S/Ag(100)

[14], and on the basis of DFT alone for S/Ag(111) [2]. These results suggest that the linear S-M-S unit has generic stability across coinage metals. This is thus a new, complementary principle for understanding and predicting stability of S-induced structures on metal surfaces.

5. Role of Cu_2S_3 complexes in Cu mass transport.

The remaining issue to be addressed is the role of the Cu_2S_3 complex in mass transport, relative to other complexes. For a realistic analysis, one must consider a coupled set of non-linear steady-state reaction-diffusion equations (RDEs) describing the formation, dissociation, and diffusion of various possible complexes [10,12]. Given that CuS_3 is reasonably stable and is a natural precursor to Cu_2S_3, we focus on the reaction $Cu + CuS_3 \leftrightarrow Cu_2S_3$, and let F (R) denote the rate for the forward (reverse) process. Then, one obtains

$$D_{Cu}\nabla^2\theta_{Cu} - F(Cu+CuS_3) + R(Cu+CuS_3) - \ldots \approx 0,$$
$$D_{Cu2S3}\nabla^2\theta_{Cu2S3} + F(Cu+CuS_3) - R(Cu+CuS_3) + \ldots \approx 0, \quad \ldots \qquad (3)$$

where D is the diffusion coefficient, and implicit terms account for contributions from other reactions. A typical feature of surface mass transport is that it is driven by weak spatial variations (and accompanying gradients) in coverages relative to their uniform quasi-equilibrium values. Thus, it is natural to write $\theta_{Cu} = \theta_{Cu}^{eq} + \delta\theta_{Cu}$, etc., and to linearize the above RDE, which results in equations of the form

$$\nabla^2 \delta\theta_{Cu} - \delta\theta_{Cu}/L_{Cu}(CuS_3)^2 + \ldots \approx 0$$
$$\text{with } L_{Cu}(CuS_3) = [D_{Cu}/k_{Cu}(CuS_3)]^{1/2} \text{ and } k_{Cu}(CuS_3)=(D_{Cu}+D_{CuS3})\theta_{CuS3}^{eq}, \text{ etc.} \qquad (4)$$

DFT indicates that $D_{Cu} >> D_{CuS3}$, so one has

$$L_{Cu}(CuS_3) \approx [\theta_{CuS3}^{eq}]^{-1/2} \text{ with } \theta_{CuS3}^{eq} = \exp[-\beta E_{form}(CuS_3)](\theta_S)^3 \qquad (5)$$

where $L_{Cu}(CuS_3)$ is the reaction length describing how far Cu diffuses before reacting with CuS_3 to form Cu_2S_3 at rate k_{Cu}.

Further analysis of behavior requires specification of the conditions under which complexes form. In one scenario, complexes are formed by Cu and S *on terraces;* only Cu adatoms detach/attach at step edges, without any barrier except the terrace diffusion barrier. However, in order for complexes to contribute to mass transport, there must be sufficient probability that they form on the terraces within a length scale much shorter than the average mass transport distance, L_{av}. In other words, any gradient in θ_{Cu} must couple sufficiently to that of θ_{Cu2S3}. From (4), this requires that the reaction length be significantly smaller than the average mass transport distance. Then there is an enhanced flux $J_{Cu2S3} \sim D_{Cu}\theta_{Cu}^{eq}/L_{Cu}$ in the presence of S, vs. $J_{Cu} \sim D_{Cu}\theta_{Cu}^{eq}/L_{av}$ without S.

To give a concrete example, consider the model case of sulfur-enhanced Cu island coarsening on Cu(111), where the transport distance becomes the island separation. Under the experimental conditions used by Ling et al. [10], $L_{av} \approx 1$ μm. This is a factor of 10 smaller than the reaction length $L_{Cu}(CuS_3) \approx 10$ μm, calculated from Eq. (5) using T = 490 K [10], $\theta_S \approx 6 \times 10^{-3}$ ML [10], and $E_{form}(CuS_3) = +0.24$ eV as given in Table 1. Hence, a diffusing Cu atom is far more likely to be captured by a Cu island than it is to form a complex on the terrace.

Thus, this picture does not allow enhanced mass transport by Cu_2S_3 *formed on terraces*. If the carrier is Cu_3S_3 formed from the reaction $Cu+Cu_2S_3 \leftrightarrow Cu_3S_3$ on terraces, a similar analysis shows that $L_{Cu}(Cu_2S_3)$ far exceeds L_{isl}, so mass transport cannot be dominated by Cu_3S_3 formed on terraces, either. Again, even if $L_{Cu}(Cu_2S_3)$ was below L_{isl}, the corresponding enhanced flux J_{Cu2S3} would scale like $(\theta_S)^{3/2}$, contrasting experiment [10].

We propose an alternative picture where complexes attach and detach directly from step edges and their coverage at step edges is determined by their local chemical potential, which depends on step edge curvature. Then they directly contribute to mass transport, and the associated mass current of a complex C can be estimated from $J_C \sim D_C\, \theta_C^{eq} \sim \exp[-E_{OR}(C)/(k_BT)]$ where $E_{OR}(C)=E_d(C)+E_{form}(C)$. Thus, the species with the lowest E_{OR} should dominate mass transport. Values of E_d and E_{form} for the clusters can be taken from Fig. 3 and Eq. (2), and for Cu atoms from Ref. [30]. This leads to values of E_{OR} = 0.91 eV, 0.49 eV, 0.46 eV, and 0.60 eV for Cu, CuS_2, Cu_2S_3, and Cu_3S_3, respectively. Therefore Cu_2S_3 should be the dominant mass carrier, with CuS_2 also playing a possible role. The above expression for the mass current due to Cu_2S_3 is consistent with the observed third-order kinetics in the S-coverage using that $\theta_{Cu2S3}^{eq}= \exp[-\beta E_{form}(Cu_2S_3)](\theta_S)^3$. We also note the likelihood that there is an extra attachment barrier inhibiting the decomposition of Cu_2S_3 at S-decorated step edges and incorporation of the Cu. This would explain the attachment-limited kinetics observed in experiment [10].

6. Conclusions.

In summary, the predominant S-induced features on the Cu(111) terraces, at very low S coverages, are heart-shaped protrusions. DFT supports their assignment as Cu_2S_3 clusters. These clusters are always oriented such that the lobes of the heart point toward downgoing B-steps, because this allows one S atom in the cluster to bond at a p4fh site. This is different than any type of metal-sulfur surface complex observed previously, to our knowledge. It may reflect the stability of linear S-metal-S geometries. Kinetic analysis shows that Cu_2S_3 is more important than Cu_3S_3 in mass transport.

Acknowledgements

The experimental component of this work was supported by several sources. From the U.S., it was NSF Grants CHE-1111500 and CHE-1507223. From Japan, support was provided by a Grant-in-Aid for Scientific Research on Priority Areas “Electron Transport Through a Linked Molecule in Nano-scale”; and a Grant-in-Aid for Scientific Research(S) “Single Molecule Spectroscopy using Probe Microscope” from the Ministry of Education, Culture, Sports, Science, and Technology (MEXT). The theoretical analysis of kinetics was also supported by NSF Grants CHE-1111500 and CHE-1507223. The DFT analysis of the energetics of chemisorbed complexes and of simulated STM images was supported by the Division of Chemical Sciences, Basic Energy Sciences, US Department of Energy (USDOE), and it utilized resources of the National Energy Research Scientific Computing Center, which is supported by the Office of Science of the US Department of Energy (Contract No. DE-AC02-05CH11231). The theoretical molecular orbital analysis for gas phase species was supported by the National Science Foundation under Grant No. CHE-1213771. C.M.A. also thanks the Camille and Henry Dreyfus Foundation for a Camille Dreyfus Teacher-Scholar Award (2011−2016). We thank Kan Ueji and Hiroshi Imada for assistance with the experiments, and Gordon J. Miller for useful discussions.

Additional Information

The authors declare no competing financial interests. Correspondence should be addressed to P.A.T.

[*]*Corresponding author:* pthiel@iastate.edu
[†]*Current address:* Ulsan National Institute of Science and Technology, South Korea

References

[1] P. J. F. Harris, Int. Mat. Rev. **40**, 97 (1995).
[2] P. A. Thiel, M. Shen, D.-J. Liu, and J. W. Evans, J. Vac. Sci. Technol. A **28**, 1285 (2010).
[3] G. S. Parkinson, Z. Novotny, G. Argentero, M. Schmid, J. Pavelec, R. Kosak, P. Blaha, and U. Diebold, Nature Materials **12**, 724 (2013).
[4] G. L. Kellogg, Phys. Rev. B **55**, 7206 (1997).
[5] S. Horch, H. T. Lorensen, S. Helveg, E. Laegsgaard, I. Stensgaard, K. W. Jacobsen, J. K. Norskov, and F. Besenbacher, Nature **398**, 134 (1999).
[6] A. R. Layson and P. A. Thiel, Surf. Sci. **472**, L151 (2001).
[7] A. R. Layson, J. W. Evans, and P.A.Thiel, Phys. Rev. B **65**, 193409 (2002).
[8] P. Maksymovych, O. Voznyy, D. B. Dougherty, D. C. Sorescu, and J. T. Yates Jr., Prog. Surf. Sci. **85**, 206 (2010).
[9] P. J. Feibelman, Phys. Rev. Lett. **85**, 606 (2000).
[10] W. L. Ling, N. C. Bartelt, K. Pohl, J. de la Figuera, R. Q. Hwang, and K. F. McCarty, Phys. Rev. Lett. **93**, 166101 (2004).
[11] K. Morgenstern, E. Laegsgaard, and F. Besenbacher, Surf. Sci. **602**, 661 (2008).
[12] M. Shen, D.-J. Liu, C. J. Jenks, P. A. Thiel, and J. W. Evans, J. Chem. Phys. **130**, 094701 (2009).
[13] M. Shen, D.-J. Liu, C. J. Jenks, and P. A. Thiel, Surf. Sci. **603**, 1486 (2009).
[14] M. Shen, S. M. Russell, D.-J. Liu, and P. A. Thiel, J. Chem. Phys. **135**, 154701 (2011).
[15] M. Foss, R. Feidenhans'l, M. Nielsen, E. Findeisen, T. Buslaps, R. I. Johnson, F. Besenbacher, and I. Stensgaard, Phys. Rev. B **50**, 8950 (1994).
[16] M. Foss, R. Feidenhans'l, M. Nielsen, E. Findeisen, T. Buslaps, R. L. Johnson, and F. Besenbacher, Surf. Sci. **388**, 5 (1997).
[17] S. M. Russell, Y. Kim, D.-J. Liu, J. W. Evans, and P. A. Thiel, J. Chem. Phys. **138**, 071101 (2013).
[18] E. Wahlström, I. Ekvall, H. Olin, S. A. Lindgren, and L. Wallden, Phys. Rev. B **60**, 10699 (1999).
[19] E. Wahlström, I. Ekvall, T. Kihlgren, H. Olin, S. A. Lindgren, and L. Wallden, Phys. Rev. B **64**, 155406 (2001).
[20] G. Kresse and J. Furthmüller, Comput. Mater. Sci. **6**, 15 (1996).
[21] P. E. Blöchl, Phys. Rev. B **50**, 17953 (1994).
[22] J. P. Perdew, K. Burke, and M. Ernzerhof, Phys. Rev. Lett. **77**, 3865 (1996).
[23] J. Tersoff and D. R. Hamann, Phys. Rev. Lett. **50**, 1998 (1983).
[24] J. Tersoff and D. R. Hamann, Phys. Rev. B **32**, 805 (1985).
[25] G. te Velde, F. M. Bickelhaupt, E. J. Baerends, C. Fonseca Guerra, S. J. A. van Gisbergen, J. G. Snijders, and T. Ziegler, J. Comput. Chem. **22**, 931 (2001).
[26] E. van Lenthe, E. J. Baerends, and J. G. Snijders, J. Chem. Phys. **101**, 9783 (1994).
[27] E. van Lenthe, A. Ehlers, and E.-J. Baerends, J. Chem. Phys. **110**, 8943 (1999).
[28] H. Häkkinen, Nature Chemistry **4**, 443 (2012).
[29] P. D. Jadzinsky, G. Calero, C. J. Ackerson, D. A. Bushnell, and R. D. Kornberg, Science **318**, 430 (2007).
[30] D.-J. Liu, Phys. Rev. B **81**, 035415 (2010).

Figure Captions

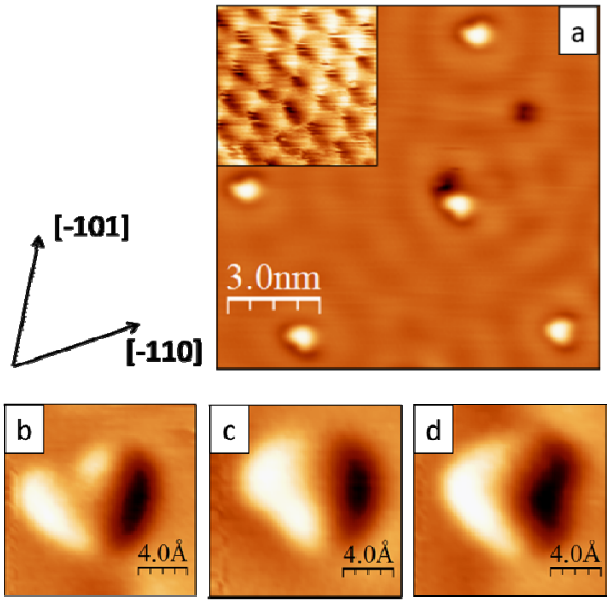

Fig. 1. STM images of Cu_2S_3 on Cu(111). a) Several Cu_2S_3 hearts on the terrace at low sulfur coverage, 12 x 11.5 nm^2, I = 1.241 nA, V_S = -2.000 V, inset: atomic resolution of clean Cu(111); 1.2 x 1.2 nm^2, I = 1.717 nA, V_S = -0.004 V. b)-d) Derivative images of the three orientations of the hearts, 1.5 x 1.5 nm^2 b) I = 1.167 nA, V_S = -0.004 V c) I = 1.292 nA, V_S = -0.020 V d) I = 1.055 nA, V_S = -0.050 V.

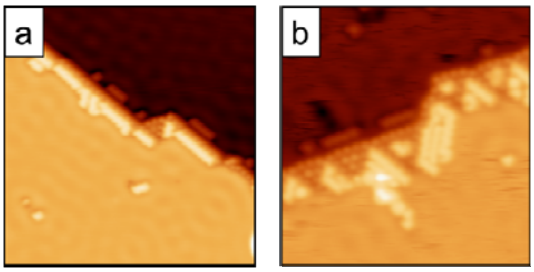

Fig. 2. Topographic STM images of the two step edge types with S adsorption. a) A-type (100-microfacet) edge; 20 x 20 nm^2, I = 1.241 nA, V_S = -0.002 V. b) B-type (111-microfacet) edge; 15 x 15 nm^2, I = 0.648 nA, V_S = -0.050 V.

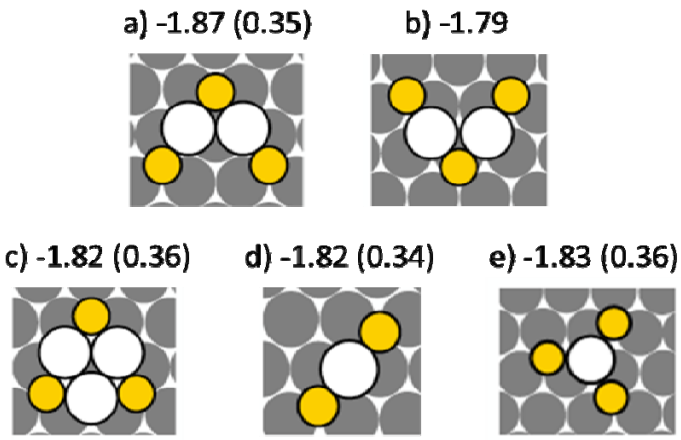

Fig. 3. Cu-S clusters on Cu(111) with lowest chemical potentials. Values of μ_S are given in eV. Diffusion barriers, E_d, are given in parentheses, also in eV. White circles represent Cu adatoms, small yellow (on-line) are S adatoms, and gray are Cu atoms in the Cu(111) surface. Panels (a) and (b) are different configurations of Cu_2S_3, (c) is Cu_3S_3, (d) CuS_2, and (e) CuS_3.

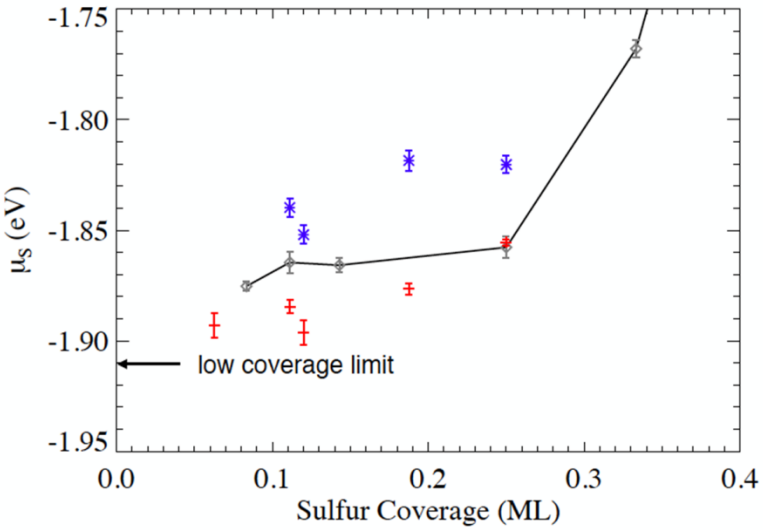

Fig. 4. Comparison between μ_S for Cu_2S_3 (red pluses) and Cu_3S_3 (blue asterisks) with that of S adatom (gray line and gray circles) on fcc sites of the Cu(111) surface. Results for various supercell sizes and azimuthal orientations are plotted as a function of S coverage.

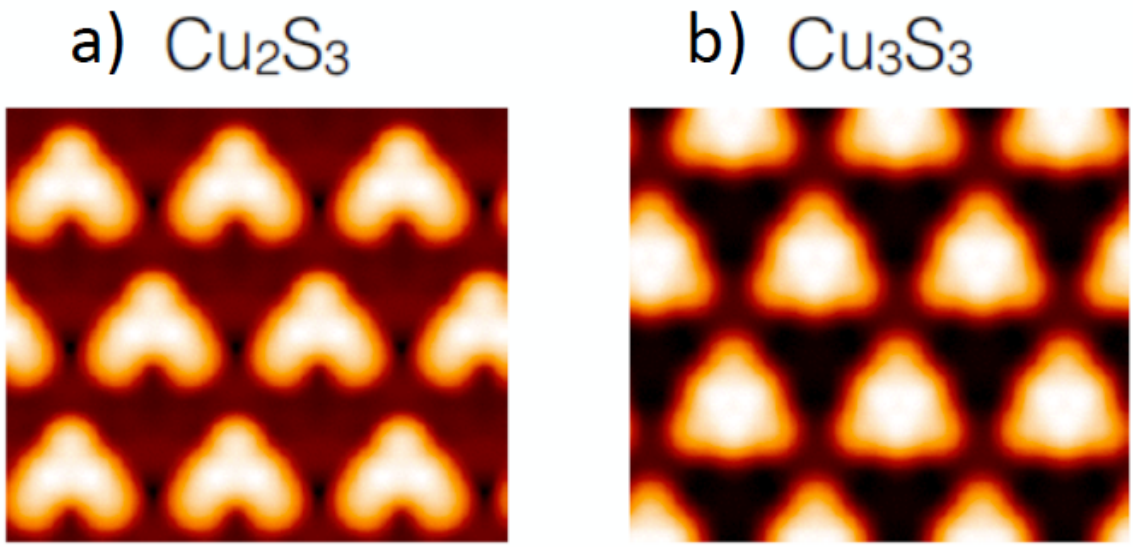

Fig. 5. Shapes of two complexes, Cu_2S_3 and Cu_3S_3 on Cu(111), simulated from DFT.

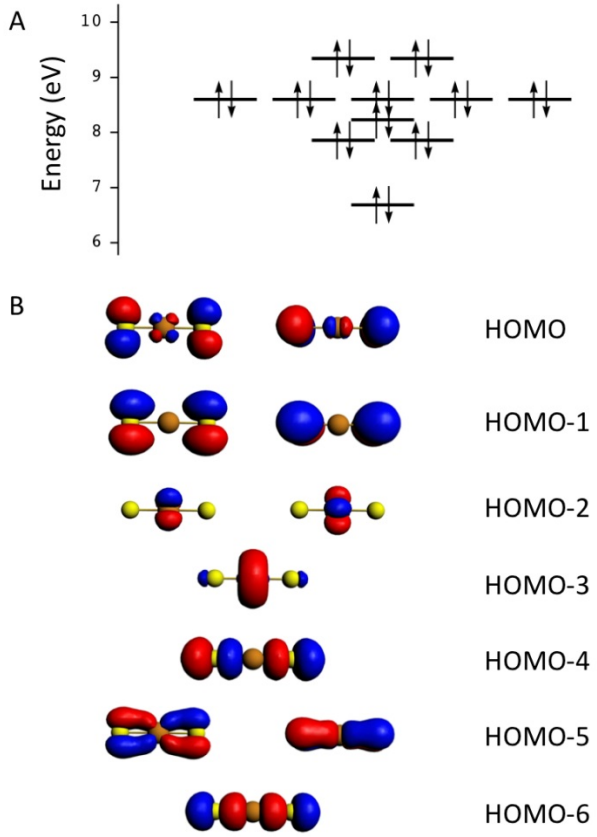

Fig. 6. A) PBE/TZP orbital energy diagram and B) Kohn-Sham orbitals for CuS_2^{3-}.

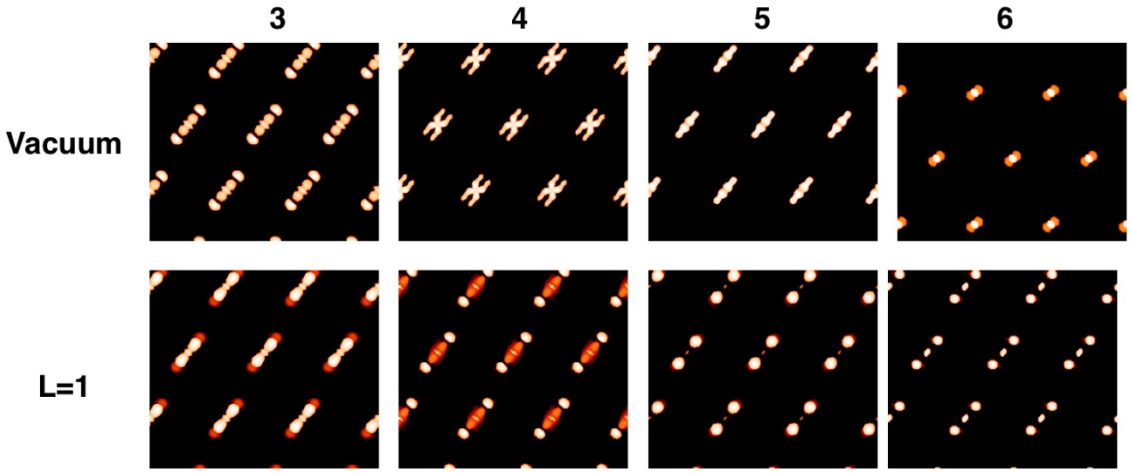

Fig. 7. VASP isodensity plots for low energy bonding states of CuS_2 in vacuum and on one layer (L=1) of Cu substrate.

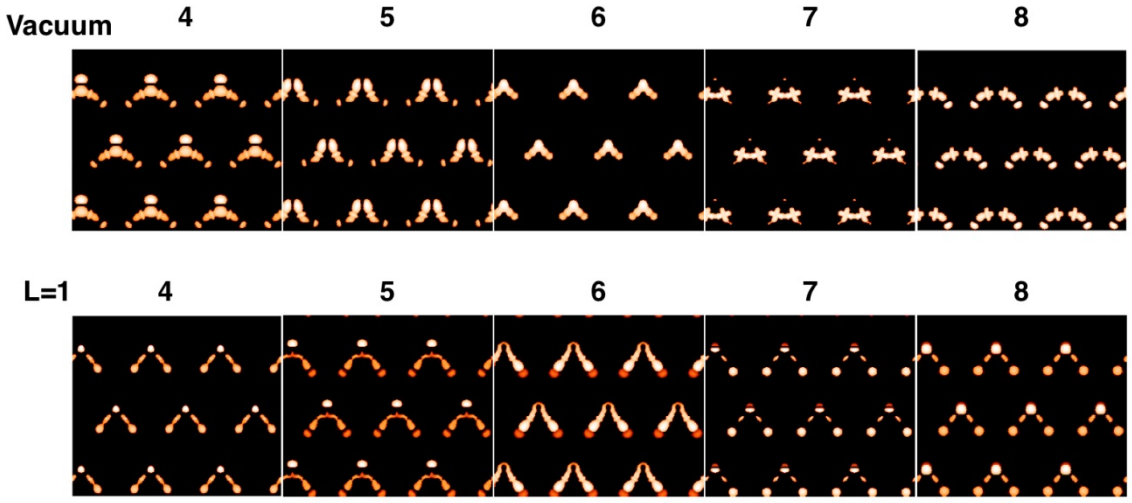

Fig. 8. VASP isodensity plots for low energy bonding states of Cu_2S_3 in vacuum and on one layer (L=1) of Cu substrate.